Evaluating uncertainty in mapping forest carbon with airborne LiDAR

Joseph Mascaro [a,b,*], Matteo Detto [b], Gregory P. Asner [a], Helene C. Muller-Landau [b]

[a] Department of Global Ecology, Carnegie Institution for Science, Stanford, CA, USA
[b] Smithsonian Tropical Research Institute, Apartado 72, Balboa, Panama

ARTICLE INFO

ABSTRACT

Airborne LiDAR is increasingly used to map carbon stocks in tropical forests, but our understanding of mapping errors is constrained by the spatial resolution (i.e., plot size) used to calibrate LiDAR with field data (typically 0.1–0.36 ha). Reported LiDAR errors range from 17 to 40 Mg C ha^{-1}, but should be lower at coarser resolutions because relative errors are expected to scale with (plot area)$^{-1/2}$. We tested this prediction empirically using a 50-ha plot with mapped trees, allowing an assessment of LiDAR prediction errors at multiple spatial resolutions. We found that errors scaled approximately as expected, declining by 38% (compared to 40% predicted from theory) from 0.36- to 1-ha resolution. We further reduced errors at all spatial resolutions by accounting for tree crowns that are bisected by plot edges (not typically done in forestry), and collectively show that airborne LiDAR can map carbon stocks with 10% error at 1-ha resolution — a level comparable to the use of field plots alone.

© 2011 Elsevier Inc. All rights reserved.

1. Introduction

Future climate change mitigation policy will likely encourage nations to reduce emissions from deforestation and degradation (REDD) by protecting and increasing forest carbon storage (Herold & Skutsch, 2011). Implementation of REDD will require large-scale, high-resolution, and verifiable approaches to monitoring above-ground tropical forest carbon stocks, which are the largest of any biome (Fischlin et al., 2007). Airborne LiDAR is one of the most promising methods; it can be applied across large regions at relatively low cost compared to field sampling alone (Asner, 2009).

The use of airborne LiDAR data, whether for purely scientific research purposes or in the policy and economic arena, requires a quantitative understanding of the errors associated with LiDAR-based carbon maps. Reported errors range from 17 to more than 40 Mg C ha^{-1} (RMSE) in the tropics (Asner et al., 2010, 2011; Mascaro et al., 2011), and are comparable in other biomes (Lefsky et al., 2002). However, these errors apply to the calibration step (i.e., the ability of LiDAR to predict the carbon density of a set of field inventory plots as assessed by a regression model), and not necessarily to carbon maps produced by such regressions. Calibration errors can be associated with mapped (predicted) carbon only if the mapping resolution (or grain) is the same as the plot size, which in existing studies ranges from 0.1 to 0.36 ha. Asner et al. (2010) noted that predicted carbon error should decline as spatial resolution decreases, because total errors increase at a slower rate than total carbon. Specifically,

Asner et al. (2010) predicted that errors should be proportional to (pixel size)$^{-1/2}$, in accordance with the general influence of sample size on the standard error of the mean. This means that typical mature forest errors of 18 Mg C ha^{-1} at a plot size of 0.36 ha would be expected to decline by 40% when decreasing spatial resolution to 1 ha. Here, we evaluate mapping errors at various spatial resolutions by correlating field-based above-ground carbon density (ACD) data to airborne LiDAR data at multiple field-plot sizes.

In addition to the tendency of error to decrease with increasing grain size, there are three sources of error that may influence the relationship between LiDAR and field-estimated carbon density at all spatial resolutions: (1) GPS positional error, (2) temporal differences between the field and LiDAR data, and (3) disagreement between LiDAR and field plot measurements over which trees or parts of trees are inside calibration plots. In LiDAR measurements, tree crowns are bisected exactly at the plot edge, while in field plot measurements, trees are treated as being inside plots if and only if >50% of the rooted base of the tree is contained within the plot (e.g., Condit, 1998). Errors of the first type were assessed on a per-plot basis in one tropical study by Asner et al. (2009) and found to be very low: adding simulated GPS errors of several meters changed plot-specific carbon estimates by less than 5 Mg C ha^{-1} for all plots, and less than 1 Mg C ha^{-1} for more than half of the plots. Temporal errors can be minimized by conducting field and LiDAR campaigns simultaneously (which is typically attempted, Asner et al., 2009, 2010, 2011). Errors of type three (differing plot edge discrimination between LiDAR and foresters) have not been empirically evaluated in any LiDAR carbon mapping study to our knowledge. However, Nelson et al. (2000) speculated that poor LiDAR prediction of ground-based ACD (90% error) in very narrow plots (5 m) was partly the result of the exclusion in the ground data of overhanging tree crowns

* Corresponding author at: Department of Global Ecology, Carnegie Institution for Science, 260 Panama St., Stanford, CA 94305, USA. Tel.: +1 650 462 1047x217; fax: +1 650 462 5968.
E-mail address: jmascaro@stanford.edu (J. Mascaro).

captured by LiDAR. Allometric errors associated with field estimates for ACD are as high as 78% of individual trees and 22% for the choice of allometric model (Chave et al., 2004); these errors were not considered here because they apply to all carbon estimates, including those used to calibrate airborne LiDAR (e.g., Asner et al., 2010), whereas we were interested in errors that apply specifically to LiDAR-based carbon mapping.

In this study, we sought to develop a better understanding of the errors in LiDAR predictions of aboveground forest carbon through two analyses of airborne LiDAR and ground inventory data for the 50-ha forest dynamics plot on Barro Colorado Island (BCI), Panama, where each stem ≥1 cm diameter is mapped to the nearest 10 cm accuracy. First, we tested the prediction of Asner et al. (2010) that spatial errors would scale with the inverse of the square root of pixel area as spatial resolution changes. Second, we tested the importance of plot-edge discrimination errors using a novel approach to ground-based determination of the position of standing carbon in forests. In typical practice, field inventories place carbon in space according to the x and y coordinates of the center of each stem, which we term the "stem-localized" approach. An alternative is to distribute carbon in space according to the footprint of the tree's crown, hereafter the "crown-distributed" approach. LiDAR is likely to be linked more closely to crown-distributed carbon density because LiDAR energy is returned more strongly by canopy material oriented perpendicular to the sensor (such as leaves and branches), rather than by tree boles that are oriented toward the sensor. Therefore, we developed crown-distributed maps of carbon density using an allometric relationship between tree diameter and crown radius developed from field data for the same site (Bohlman & O'Brien, 2006), and evaluated LiDAR mapping errors with respect to both the stem-localized and crown-distributed maps.

2. Methods

In September 2009, we used the Carnegie Airborne Observatory (Asner et al., 2007) to collect LiDAR data over the 50-ha forest dynamics plot on BCI (9° 9′ N, 79° 50′ W) (Mascaro et al., 2011). Forests on BCI are tropical moist (Holdridge et al., 1971), with 2600 (±430) mm of rainfall annually with a pronounced dry season between January and April (<100 mm per month, Leigh, 1999). The LiDAR data were collected with an Optech 3100EA (Optech Inc., Vaughan, ON), capable of four returns per pulse, with beam divergence customized to 0.56 mrad (for complete coverage without gaps between pulses). The system was operated at 2000 m above ground level with 1.12-m spot spacing, 30-degree field of view, and 50-kHz pulse repetition frequency, for which the aircraft maintained a ground speed ≤157 kph. Flights were planned with 100% repeat coverage (50% overlap of each swath to each adjacent swath) and therefore LiDAR point density averaged 2 points per 1.12-m spot. We analyzed the vertical profile of vegetation by binning discrete LiDAR point-cloud data into volumetric pixels (voxels) of 5-m spatial resolution and 1-m vertical resolution. By combining all voxels in each 5×5 m spatial cell, we created vertical histograms representing the full vertical spread of LiDAR returns. These data were broken down to mean canopy profile height (i.e. MCH, the vertical "center" of the canopy), a simple metric to be linked to ground data (Lefsky et al., 1999). Although several LiDAR metrics strongly predict forest carbon density, MCH is slightly but consistently better than top-of-canopy height or alternative LiDAR-based indices, such as quadratic mean canopy height (Asner et al., 2011).

LiDAR MCH data were previously calibrated to field-based estimates of aboveground carbon density (ACD measured in 2009–2010) in 128, 60×60 m quadrats within the 50-ha plot combined with 29, 20×50 m transects in younger forests in the Panama Canal Zone (Mascaro et al., 2011). Field-estimated ACD was determined for all living trees >1 cm dbh using a combination of local and global allometric models that corrected for local height and wood density variation (Mascaro et al., 2011), producing an overall carbon estimate for the 50-ha plot of 107 Mg C ha^{-1}, which is very close to another recent estimate of 103 Mg C ha^{-1} (DeWalt & Chave, 2004). For the MCH-ACD relationship, 60×60 m quadrats

(0.36 ha) were chosen to best match previous plot sizes (~0.28 ha) used in closed canopy mainland tropical forests (Asner et al., 2010). This calibration yielded a power-law model between ACD and MCH:

$$ACD = 1.4110*MCH^{1.4126} \tag{1}$$

which explained 85% of the variation in ACD with an RMSE of 16.6 Mg C ha^{-1}. For the 60×60 m quadrats in mature forest, the RMSE was 18.0 Mg C ha^{-1}.

We used the published model to generate predictions of ACD from LiDAR across 22 spatial resolutions within the 50-ha plot, from 0.04 to 12.5 ha. We used only the 22 native resolutions that utilized 100% of the area within the 50-ha plot, including 17 that were rectangular rather than square (Supplementary material, Table S1). We considered the influence of differing plot shape, and found it to be very low (1.5 Mg C ha^{-1}), especially for the range of length-to-width ratios that we use to compare across scales (Supplementary material, Figure S1). We compared errors across all resolutions with respect to the previously published model rather than refitting the model at each resolution because the secondary forests plots originally used by Mascaro et al. (2011) were noncontiguous and therefore not combinable. We verified that this limitation did not impact the overall pattern (Supplementary material).
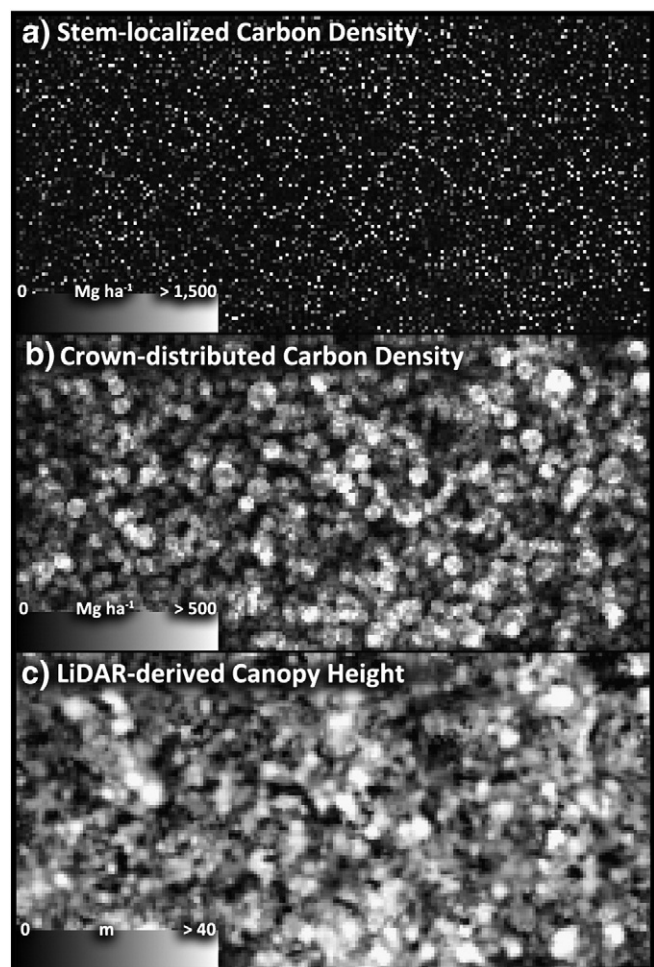
Fig. 1. Spatial organization of carbon in 5×5 m cells in the 50-ha forest dynamics plot on Barro Colorado Island, Panama. Ground-based estimates of carbon density are shown when each tree's carbon is (a) assigned to the position of its stem, and (b) distributed uniformly over its estimated crown area, drawn as a circle around the position of the stem, with radius estimated from diameter using an allometric model. LiDAR-derived canopy height (c) is shown for comparison.
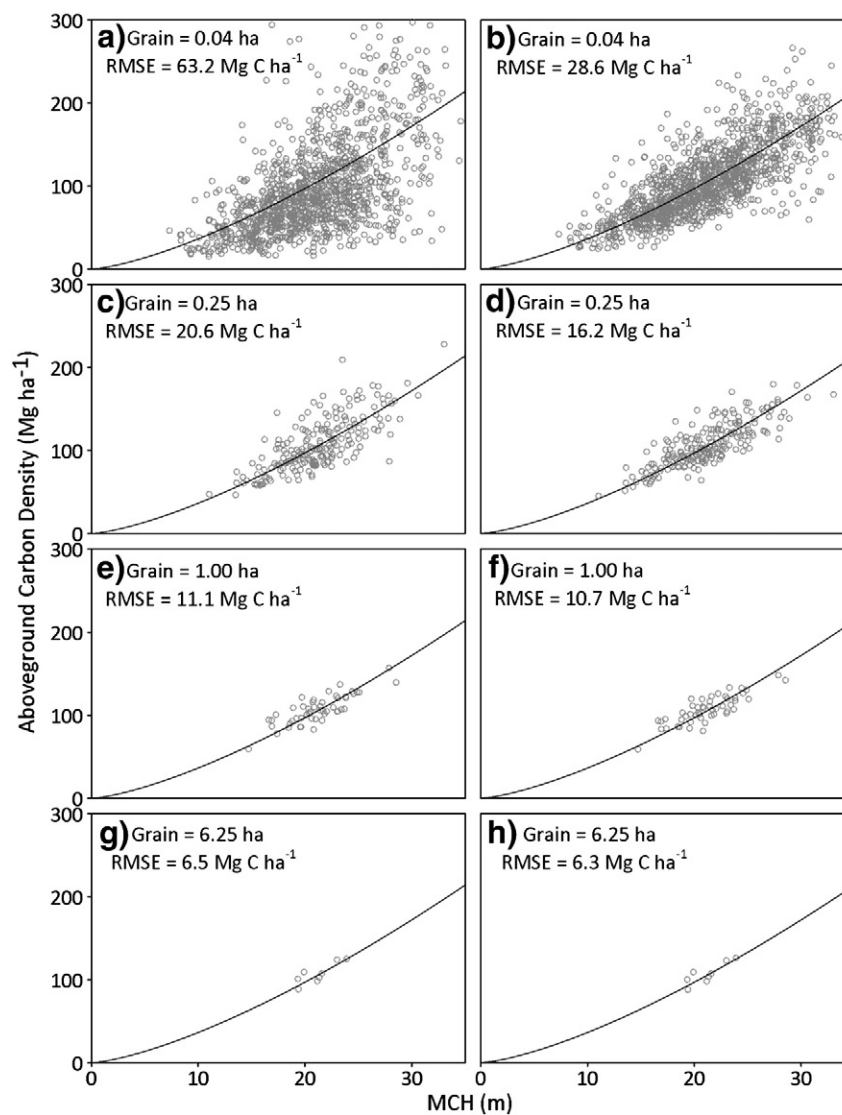
Fig. 2. Error in LiDAR-based carbon density prediction in the 50-ha forest dynamics plot on Barro Colorado Island, Panama, for a range of spatial resolutions, in comparison with ground-based estimates calculated using stem-localized (a, c, e, g) and crown-distributed (b, d, f, h) approaches. Predictions at all resolutions were derived from LiDAR-measured MCH using a model fitted at 0.36-ha resolution by Mascaro et al. (2011). Several points are outside the range of panels (a) and (b) to allow the bulk of the points to be compared on standardized axes.

Across the resolutions of interest, we compared LIDAR predictions with two different ground-based estimates of ACD: (1) stem-localized ACD, in which the carbon estimated for a single stem is positioned at the x, y coordinates of the center of that stem (i.e., the typical approach used in long-term forest inventory and biomass monitoring; Fig. 1a), and (2) crown-distributed ACD, in which the carbon estimated for each stem is distributed on a circle representing the stem's crown (Fig. 1b). In the latter case, estimated carbon within a given cell at a given resolution (e.g., a 20×20 m quadrat) was the sum of all circular crown footprints (on a proportional basis) that occupy that cell. Crown radii were estimated from stem diameter using an allometric model developed for the Barro Colorado Nature Monument by Bohlman and O'Brien (2006):

$$R = \exp(-0.438 + 0.658^*\log(D/10)) \qquad (2)$$

where R is radius (m) and D is diameter at breast height (1.3 m) or above buttress. All analyses were conducted in the R programming language (R Development Core Team, 2009).

3. Results and discussion

As expected, LiDAR predictive power increased strongly with decreasing spatial resolution (Figs. 2 and 3). From 0.04- to 6.25-ha resolution, RMSE of observed carbon density as predicted by LiDAR decreased from 63.2 to 6.5 Mg C ha^{-1} (Fig. 2, left panels). We also found that LiDAR data predictions were a much closer match to crown-distributed carbon density than to stem-localized carbon density, particularly at finer spatial resolutions (Fig. 2, right panels). At 0.04-ha resolution, RMSE dropped from 63.2 to 28.6 Mg C ha^{-1} when considering crown-distributed rather than stem-localized carbon density (Fig. 2a versus b).

RMSE of stem-localized carbon density declined as predicted by Asner et al. (2010) for grain sizes from 0.08 to 1 ha, but decreased slightly faster than predicted at resolutions finer than 0.08 ha, and considerably slower than predicted at resolutions coarser than 1 ha (Fig. 3). By contrast, RMSE of crown-distributed carbon density declined at a much slower rate than predicted until ~1 ha, after which stem-localized and crown-distributed carbon RMSE essentially converged. Deviations from the theoretical prediction at resolutions finer
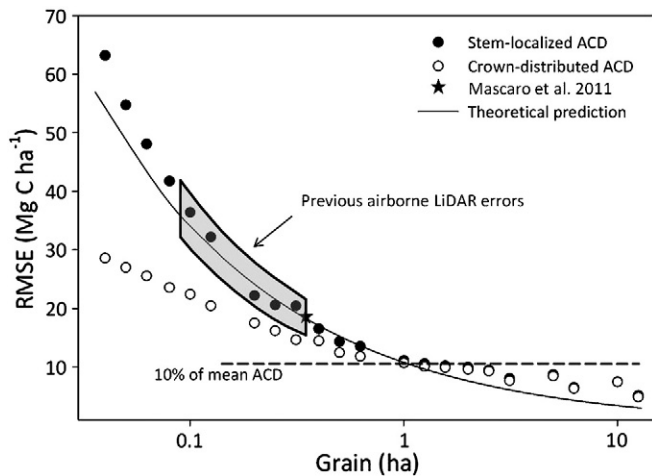
Fig. 3. Observed decline in LiDAR-based carbon density prediction error with decreasing spatial resolution in the 50-ha forest dynamics plot on Barro Colorado Island, Panama, using stem-localized and crown-distributed aboveground carbon density estimates (ACD), compared with the theoretical expectation that errors should decline with (grain size)$^{-1/2}$ (Asner et al., 2010). The calibration grain size is 0.36 ha (Mascaro et al., 2011).

than 1 ha reflect spatial autocorrelation in the carbon errors; these are slightly negative for stem-localized carbon and strongly positive for crown-distributed carbon (Supplementary material, Figure S2). At resolutions coarser than 1 ha, the declining number of plots increases the importance of a small amount of net error (~1 Mg C ha^{-1}) caused by the fact that the original calibration equation is leveraged in part by secondary forest data not considered here (see Methods). The departure may also reflect large-scale positive spatial autocorrelation in errors caused by variation in forest structure (i.e., gaps), but the limited number of plots precludes testing this hypothesis at present. Although predicted errors departed from theoretical predictions at very coarse resolutions, they continued to decline as a function of decreasing spatial resolution and remained very low relative to field errors (discussed further below).

The finding that crown-distributed carbon density was more closely related to LiDAR predictions than stem-localized carbon density is important because it demonstrates that a primary source of error at fine spatial resolutions is disagreement between what is and what is not inside a plot. In a LiDAR dataset, laser returns are spatially rectified in three dimensions, reflecting the three-dimensional nature of the forest canopy determined by the position of leaves, branches, and other material. Thus, a plot "footprint" in a LiDAR dataset is a cylinder that bisects trees based on the amount of canopy material inside the plot volume. For foresters, by contrast, >50% of a tree's bole must be contained within the plot footprint for a tree to be counted inside a plot — but the distinction is all or nothing (Condit, 1998).

In reality, carbon is distributed neither in stem-localized nor crown-distributed fashion, but something in between. A majority of carbon is stored in the bole of a tree, but approximately 30% may be distributed across the crown (Brown, 1997). Thus, it could be argued that stem-localized carbon density more closely resembles real carbon density in a forest. However, our purpose is not to delineate carbon density at the sub-tree levels: we believe such an exercise is not destined to improve policy related to carbon retention in tropical forests. Our use of crown-distributed carbon density here is merely intended to show that LiDAR is better related to crown-distributed than stem-localized carbon density — and when this relationship is used, overall LiDAR mapping errors are lower. Although we considered LiDAR and field ACD data, plot edge disagreement may also produce errors in other remote assessments of forest structure,

including radar and passive optical techniques (e.g., Foody et al., 2003; Saatchi et al., 2007).

We also detected a strong interaction between spatial resolution and the ground-based method used to map carbon density (i.e., stem-localized versus crown-distributed). We found that the benefit of using crown-distributed carbon density was greatest at the finest resolution, and decreased progressively until at 1-ha resolution these methods were roughly comparable. This reflects an increasing edge-to-interior ratio with decreasing spatial resolution: as plot size increases, the fraction of trees with portions of their crowns falling across a plot edge decreases dramatically.

For the purposes of LiDAR calibration, increasing plot sizes may reduce the application range of the calibration model as the number of data points declines. However, this occurred here because all plots considered were in mature forest (Fig. 2), which would not be the case when planning a new field calibration in a given region. Asner et al. (2010) found that ~24 plots spanning a range of forest ages were necessary to stabilize a LiDAR-ACD calibration model, and this number of 1-ha plots (24 ha total) is well below the amount of sampling conducted for recent calibrations (e.g., Asner et al., 2010, 2011).

Our results suggest that LIDAR-derived maps of mature tropical forest carbon density can achieve overall accuracy of 10% at 1-ha resolution (RMSE = 10.7 Mg C ha^{-1} relative to mature forest carbon density of ~107 Mg C ha^{-1}; Fig. 3). Because the same area was used for calibration and prediction, these results may overstate accuracy to some degree; however, region-specific LiDAR models of the type considered here have shown consistently verifiable predictive power across regions as large as 1 million hectares (e.g., Asner et al., 2010, 2011). Collectively, our results demonstrate that LiDAR mapping of carbon density can be achieved with error levels comparable to field campaigns, where landscape-scale sampling error may be 10% of the mean or greater (Chave et al., 2004). Field-based sampling of carbon density using forest inventory plots may produce landscape-scale errors of 10–20% with a total sample size of 5 ha (Clark & Clark, 2000; Keller et al., 2001), or 7% using 50 total ha of sampling in the same area considered in this study (Chave et al., 2003). These errors also depend on the size of the area sampled and the plot size used: smaller sample area produces larger errors (Chave et al., 2004), and for any given area, fewer larger plots lead to greater errors in landscape estimates (Fisher et al., 2008). Thus, our results underscore the utility of airborne LiDAR in fulfilling the ecological and policy-relevant need for understanding geographic variation in tropical forest carbon density.

Appendix A. Supplementary data

Supplementary data to this article can be found online at doi:10.1016/j.rse.2011.07.019.

References

Asner, G. P. (2009). Tropical forest carbon assessment: Integrating satellite and airborne mapping approaches. *Environmental Research Letters*, 3, 1748–9326.

Asner, G. P., Hughes, R. F., Mascaro, J., Uowolo, A., Knapp, D. E., Jacobson, J., et al. (2011). High-resolution carbon mapping on the million-hectare Island of Hawai'i. *Frontiers in Ecology and the Environment*, doi:10.1890/100179.

Asner, G. P., Hughes, R. F., Varga, T. A., Knapp, D. E., & Kennedy-Bowdoin, T. (2009). Environmental and biotic controls over aboveground biomass throughout a tropical rain forest. *Ecosystems*, 12, 261–278.

Asner, G. P., Knapp, D. E., Kennedy-Bowdoin, T., Jones, M. O., Martin, R. E., Boardman, J., et al. (2007). Carnegie Airborne Observatory: In-flight fusion of hyperspectral imaging and waveform light detection and ranging (LiDAR) for three-dimensional studies of ecosystems. *Journal of Applied Remote Sensing, 1*, doi:10.1117/1111.2794018.

Asner, G. P., Powell, G. V. N., Mascaro, J., Knapp, D. E., Clark, J. K., Jacobson, J., et al. (2010). High-resolution forest carbon stocks and emissions in the Amazon. *Proceedings of the National Academy of Sciences*, 107, 16738–16742.

Bohlman, S., & O'Brien, S. (2006). Allometry, adult stature and regeneration requirement of 65 tree species on Barro Colorado Island, Panama. *Journal of Tropical Ecology*, 22, 123–136.

Brown, S. (1997). *Estimating biomass and biomass change of tropical forests.* Rome: FAO Forestry Papers.

Chave, J., Chust, G., Condit, R., Aguilar, S., Hernandez, A., Lao, S., et al. (2004). Error propagation and scaling for tropical forest biomass estimates. *Philosophical Transactions of the Royal Society B: Biological Sciences*, 359, 409–420.

Chave, J., Condit, R., Lao, S., Casperson, J. P., Foster, R. B., & Hubbell, S. P. (2003). Spatial and temporal variation of biomass in a tropical forest: results from a large census plot in Panama. *Journal of Ecology*, 91, 240–252.

Clark, D. B., & Clark, D. A. (2000). Landscape-scale variation in forest structure and biomass in a tropical forest. *Forest Ecology and Management*, 137, 185–198.

Condit, R. (1998). *Tropical forest census plots.* Berlin: Springer-Verlag & Georgetown, Texas: R. G. Landes Company.

Dewalt, S. J., & Chave, J. (2004). Structure and biomass of four lowland neotropical forests. *Biotropica*, 36, 7–19.

Fischlin, A., Midgley, G. F., Price, J. T., Leemans, R., Gopal, B., Turley, C., et al. (2007). Ecosystems, their properties, goods, and services. In M. L. Parry, O. F. Canziani, J. P. Palutikof, P. J. Van Der Linden, & C. E. Hanson (Eds.), *Climate change 2007: Impacts, adaptation and vulnerability. Contribution of working group II to the forth assessment report of the Intergovernmental Panel on Climate Change* (pp. 211–272). Cambridge: Cambridge University Press.

Fisher, J. I., Hurtt, G. C., Thomas, R. Q., & Chambers, J. Q. (2008). Clustered disturbances lead to bias in large-scale estimates based on forest sample plots. *Ecology Letters*, 11, 554–563.

Foody, G. M., Boyd, D. S., & Cutler, M. E. J. (2003). Predictive relations of tropical forest biomass from Landsat TM data and their transferability between regions. *Remote Sensing of Environment*, 85, 463–474.

Herold, M., & Skutsch, M. (2011). Monitoring, reporting and verification for national REDD + programmes: Two proposals. *Environmental Research Letters*, 6, 014002.

Holdridge, L. R., Grenke, W. C., Hatheway, W. H., Liang, T., & Tosi, J. A., Jr. (1971). *Forest environments in tropical life zones.* New York: Pergamon Press.

Keller, M., Palace, M., & Hurtt, G. C. (2001). Biomass estimation in the Tapajos National Forest, Brazil; examination of sampling and allometric uncertainties. *Forest Ecology and Management*, 154, 371–382.

Lefsky, M. A., Cohen, W. B., Harding, D. J., Parker, G. G., Acker, S. A., & Gower, S. T. (2002). Lidar remote sensing of above-ground biomass in three biomes. *Global Ecology & Biogeography*, 11, 393–399.

Lefsky, M. A., Harding, D., Cohen, W. B., Parker, G., & Shugart, H. H. (1999). Surface lidar remote sensing of basal area and biomass in deciduous forests of Eastern Maryland, USA. *Remote Sensing of Environment*, 67, 83–98.

Leigh, E. G., Jr. (1999). *Tropical forest ecology: A view from Barro Colorado Island.* Oxford: Oxford University Press.

Mascaro, J., Asner, G. P., Muller-Landau, H. C., Van Breugel, M., Hall, J., & Dahlin, K. M. (2011). Controls over aboveground forest carbon density on Barro Colorado Island, Panama. *Biogeosciences*, 8, 1615–1629.

Nelson, R., Jimenez, J., Schnell, C. E., Hartshorn, G. S., Gregoire, T. G., & Oderwald, R. (2000). Canopy height models and airborne lasers to estimate forest biomass: Two problems. *International Journal of Remote Sensing*, 21, 2153–2162.

R Development Core Team (2009). *R: A language and environment for statistical computing.* ISBN 3-900051-07-0, URL http://www.R-project.org. Vienna: R Foundation for Statistical Computing.

Saatchi, S. S., Houghton, R. A., Alvalá, R., Soares, J. V., & Yu, Y. (2007). Distribution of aboveground live biomass in the Amazon basin. *Global Change Biology*, 13, 816–837.